Electronic Supplementary Information

Mass production of single-atom cobalt photocatalyst for high-performance visible-light photocatalytic CO_2 reduction

Pianpian Zhang,[a] Xiaoning Zhan,[a] Lianbin Xu,[b] Xianzhang Fu,[a] Tianyu Zheng,[a] Xiya Yang,[a] Qingmei Xu,[a] Danni Wang,[a] Dongdong Qi,[a] Tingting Sun*[a] and Jianzhuang Jiang*[a]

[a]*Beijing Key Laboratory for Science and Application of Functional Molecular and Crystalline Materials, Department of Chemistry, University of Science and Technology Beijing, Beijing 100083, China*

[b]*State Key Laboratory of Organic−Inorganic Composites, Beijing University of Chemical Technology, Beijing 100029, China*

*E-mail addresses: ttsun99@ustb.edu.cn (T. Sun), jianzhuang@ustb.edu.cn (J. Jiang)

CONTENTS

1. Experimental Section

1.1 Chemicals

All the reagents and solvents were of reagent grade and used as received. Commercial super conductive carbon black (SP) was purchased from TIMICAL and used directly without additional fabrication. Concentrated sulfuric acid (95%~98%) was procured from Alfa Aesar. N, N-Dimethylformamide (DMF, ≥99.5%) was purchased from Beijing Chemical works. Ethanol (EtOH, ≥99.7%) were supplied by Sinopharm Chemical Reagent Co., Ltd. Acetonitrile (MeCN, ≥99.7%), Trisopropanolamine (TIPA, ≥98.0%) and $[Ru(bpy)_3]Cl_2 \cdot 6H_2O$ (98%) were purchased from Aladdin. Iron phthalocyanine (FePc, 90%), cobalt phthalocyanine (CoPc, 95%), nickel phthalocyanine (NiPc, 93%), and copper phthalocyanine (CuPc, 93%) were purchased from Shanghai Macklin Biochemical Technology Co., Ltd. CO_2 gas of 99.995 % in purity was provided by Suzhou Jinhong Gas Co., Ltd.

1.2 Materials Characterization

Transmission electron microscopy (TEM) images were collected from HT7700 electron microscope at 100 KV. The high-angle annular dark-field scanning TEM (HAADF-STEM) images and energy dispersive X-ray spectroscopy (EDS) mapping images were taken on a JEM-ARM200F electron microscope operated at 200 kV. Atomic resolution HAADF-STEM images were acquired from a Titan 80-300 scanning/transmission electron microscope operated at 300 kV. Powder X-ray diffraction (PXRD) tests were performed on a Shimadzu XRD-6000 diffractometer using Cu-Kα radiation (λ= 1.54056 Å) at room temperature. X-ray photoelectron spectroscopy (XPS) patterns were collected from an ESCALAB 250 X-ray photoelectron spectrometer. The X-ray absorption near-edge structure (XANES) and extended X-ray absorption fine structure (EXAFS) of the sample at Co K-edge was collected at the BL14W1 station in Shanghai Synchrotron Radiation Facility (SSRF). The Co content of the Co-SA@SP-800 was determined by inductively coupled plasma

atomic emission spectroscopy (ICP-AES) analysis with an Agilent ICP-OES 725 ES instrument. The Brunauer–Emmett–Teller surface areas of the samples were analyzed from nitrogen adsorption-desorption isotherms by using a Micromeritics ASAP 2010 instrument at 77 K, the CO_2 adsorption-desorption isotherms was analyzed at 298K. UV-vis absorption spectra were recorded on a Shimadzu 3600 spectrophotometer. Photoluminescence (PL) spectra were recorded on a HITACHI F-4500 spectrophotometer, as well as the solvent was the mixture of MeCN and H_2O with volume ratio of 5:3 and the system was excited at 400 nm.

1.3 XAFS Measurement and Analysis

All the Co K-edge XAFS data were recorded in a fluorescence mode under the same ambient conditions. Co foil, CoPc, CoO and Co_3O_4 were used as references.

The collected EXAFS data were managed by the ATHENA module of the IFEFFIT software packages following the standard procedures. By deducting the post-edge background from the whole absorption spectra and then normalizing in regard to the edge-jump step, the k^3-weighted EXAFS spectra can be obtained. After that, the k^3-weighted χ (k) data were Fourier transformed to real (R) space by a hanging window (dk=1.0 $Å^{-1}$) to separate the EXAFS contributions from different coordination shells. The quantitative coordination numbers of the central Co atom were simulated using least-squares curve parameter fitting by the ARTEMIS module of IFEFFIT software packages.The following EXAFS fitting equation was used:

$$\chi(k) = \sum_j \frac{N_j S_0^2 F_j(k)}{k R_j^2} \exp[-2k^2\sigma_j^2] \exp[\frac{-2R_j}{\lambda(k)}] \sin[2kR_j + \phi_j(k)]$$

Where S_0^2 represents the amplitude reduction factor, $F_j(k)$ is the effective curved-wave backscattering amplitude, N_j is the number of neighbors in the j^{th} atomic shell, R_j is the distance between the X-ray absorbing central atom and the atoms in the j^{th} atomic shell (backscatterer), λ is the mean free path in Å, $\phi_j(k)$ is the phase shift (including the phase shift for each shell and the total central atom phase shift), σ_j is the Debye-Waller parameter of the j^{th} atomic shell (variation of distances around the average R_j). The functions $F_j(k)$, λ and $\phi_j(k)$ were calculated with the ab initio code FEFF8.2. The additional details for EXAFS simulations are given below.

The coordination numbers of the Co atoms in the Co-SA@SP-800 catalyst were fixed to the nominal values. The obtained S_0^2 was fixed in the next fitting step. The internal atomic distances R, Debye-Waller factor σ^2, and the edge-energy shift ΔE_0 were allowed to run freely.

1.4 Calculation of Turnover Number (TON)

The turnover number (TON) of Co-SA@SP-800 was calculated using the following equation:

$$TON = \frac{moles\ of\ products\ evolved}{moles\ of\ active\ components\ on\ photocatalyst}$$

Moles of products evolved: CO was detected to be the major product of CO_2 reduction, and after 2 hours of light irradiation, the amount of CO was detected to be 32.8 μmol.

Moles of active components on the photocatalyst: the loading amount of Co was determined to be 1.29 wt% by the test of ICP. Thus, the moles of active components is (0.002 g × 1.29 wt%)/59 g mol^{-1} = 0.437 × 10^{-6} mol = 0.437 μmol. Thus, TON = 32.8 μmol/0.437 μmol = 75.

1.5 The Apparent Quantum Efficiency (AQE)

The apparent quantum efficiency (AQE) is defined by the equation:

$$\varphi_x = \frac{\mp (d[x]/dt)}{d[hv]_{inc}/dt}$$

where d[x]/dt is the rate of change of the concentration of the reactant (or product) and $d[hv]_{inc}/dt$ is the total optical power impinging on the sample. Generally, for the convenient of measurement and calculation, researchers usually use the integral form of equation:

$$AQE(\%) = \frac{number\ of\ the\ electrons\ taking\ part\ in\ reaction}{number\ of\ incident\ photons} \times 100\%$$

Since CO was detected to be the major product of CO_2 reduction, and two electrons are needed to get one molecule of CO. The numerator and denominator of equation are divided by unit time simultaneously. Thus, the AQE equation can be transformed into the following formation:

$$AQE(\%) = \frac{2 \times number\ of\ evolved\ CO\ molecules/unit\ time}{number\ of\ incident\ photons/unit\ time} \times 100\%$$

We denote the numerator of equation as N_e, and the denominator of equation as N_p. Thus, the N_e means the amounts of electrons taking part in CO_2RR during the unit time, and N_p means the amounts of incident photons during the unit time, and equation can be written as:

$$AQE(\%) = \frac{N_e}{N_p} \times 100\%$$

Thus, we can calculate the AQE as long as we can get the value of N_e and N_p under the incident light with a specific wavelength. Here, we demonstrate the process with the example of AQE calculation under irradiation with the wavelength of 420 nm.

N_e: The amount of CO generated by unit catalyst at the unit time was detected under the irradiation with the wavelength of 420 nm. The generation rate of CO under 420 nm is 16.4 μmol h^{-1}, which can

be transferred to be 4.56×10^{-9} mol s^{-1}. Thus, $N_e = 2 \times 4.56 \times 10^{-9} = 9.12 \times 10^{-9}$ mol s^{-1}.

N_p: The energy of single photon (denoted as E_s) at $\lambda = 420$ nm can be calculated to be 4.730×10^{-19} J according to $E_s = (hc)/\lambda$, where h and c are the Planck constant (6.626×10^{-34} J·s) and the speed of light (2.998×10^{8} m s^{-1}), respectively. Avogadro constant (denoted as N_A) equals 6.022×10^{23} mol^{-1}. The light intensity (denoted as I_{in}) was measured to be 25.3 mW cm^{-2}, which can be transferred to be 25.3×10^{-3} J $s^{-1} \cdot cm^{-2}$. The diameter (denoted as d) of illumination window of the reactor was measured to be 5 cm, and thus the irradiation area (denoted as S_{in}) can be calculated to be 19.63 cm^2 according to the equation $S_{in} = \pi \times (d/2)^2$. Thus, the N_p can be calculated by divide the total energy provided in unit time by the energy of single photon: $N_p = (I_{in} \times S_{in}) / (E_s \times N_A) = 25.3 \times 10^{-3}$ J $s^{-1} \cdot cm^{-2} \times 19.63$ cm^2 / 4.730×10^{-19} J $\times 6.022 \times 10^{23}$ $mol^{-1} = 1.744 \times 10^{-6}$ mol s^{-1}.

Thus, according to above equation, AQE (%) = $N_e / N_p \times 100\% = 9.12 \times 10^{-9}$ mol s^{-1} / 1.744×10^{-6} mol $s^{-1} \times 100\% = 0.52\%$.

1.6 Theoretical Calculation

All the density functional theory (DFT) calculations were carried out by Guassian 09 D.01 software package. The geometry structure of each sample was constructed and optimized on the basis of M06. The accurate Gibbs free energy value of each optimized structure was calculated on the basis of the Nørskov model.

For CO_2RR calculation, the two electrons involved pathway generally proceeds according to the following steps:

(1) $* + CO_2\ (g) + H^+ + e^- \rightarrow *COOH$

(2) $*COOH + H^+ + e^- \rightarrow *CO + H_2O$

(3) $*CO \rightarrow CO\ (g) + *$

Where the asterisk (*) indicates an active site.

The Gibbs free energy change (ΔG) of CO_2RR catalyzed by Co-SA@SP-800 photocatalyst was calculated through the following equation:

$\Delta G = \Delta E + \Delta ZPE - T\Delta S$

Where ΔE is the adsorption energy of CO_2RR intermediates, and ΔZPE represents the zero-point energy. The temperature (T) in the equation was set to 298K to conform to the experiment condition. ΔS is the entropy change.

2. Supplementary Figures and Tables

Fig. S1. Photos of the large-scale production of Co-SA@SP-800 catalyst.

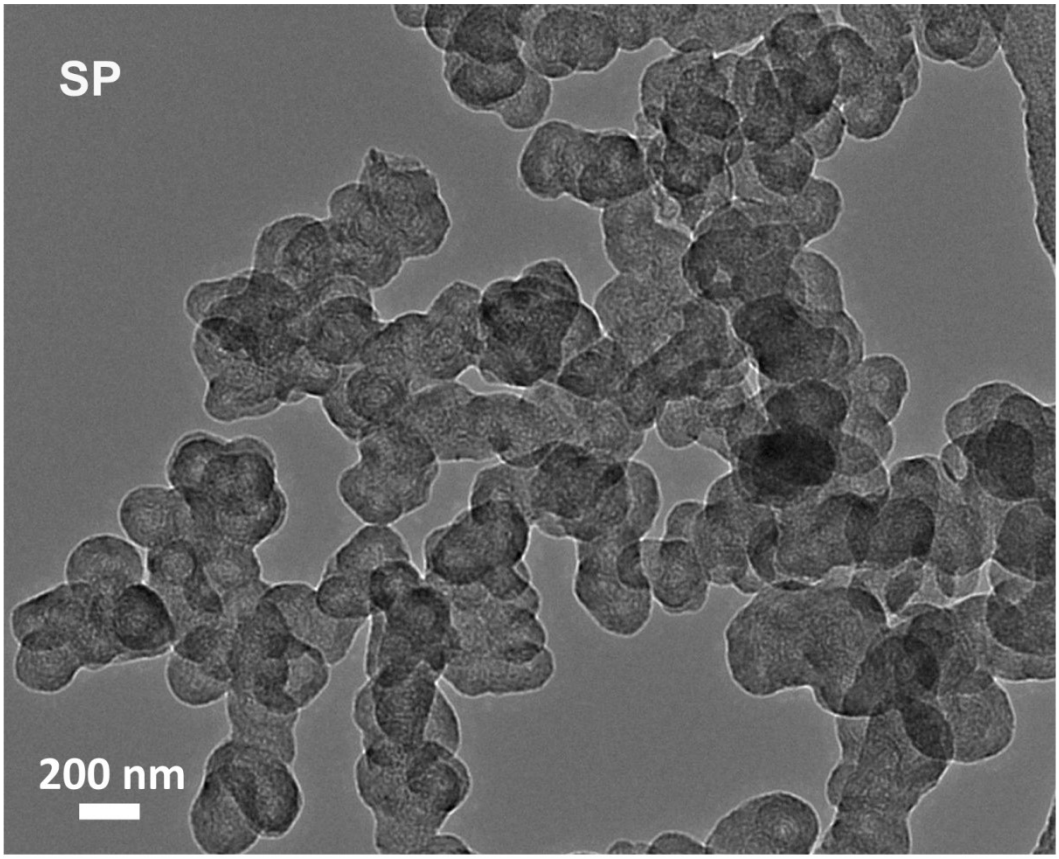

Fig. S2. TEM image of SP.

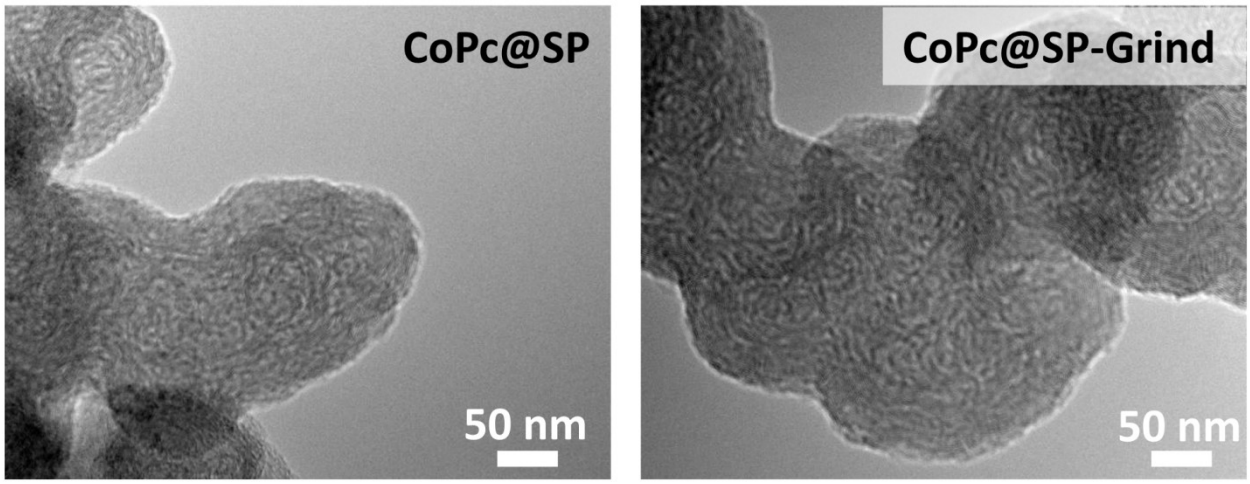

Fig. S3. TEM images of CoPc@SP (left) and CoPc@SP-Grind (right).

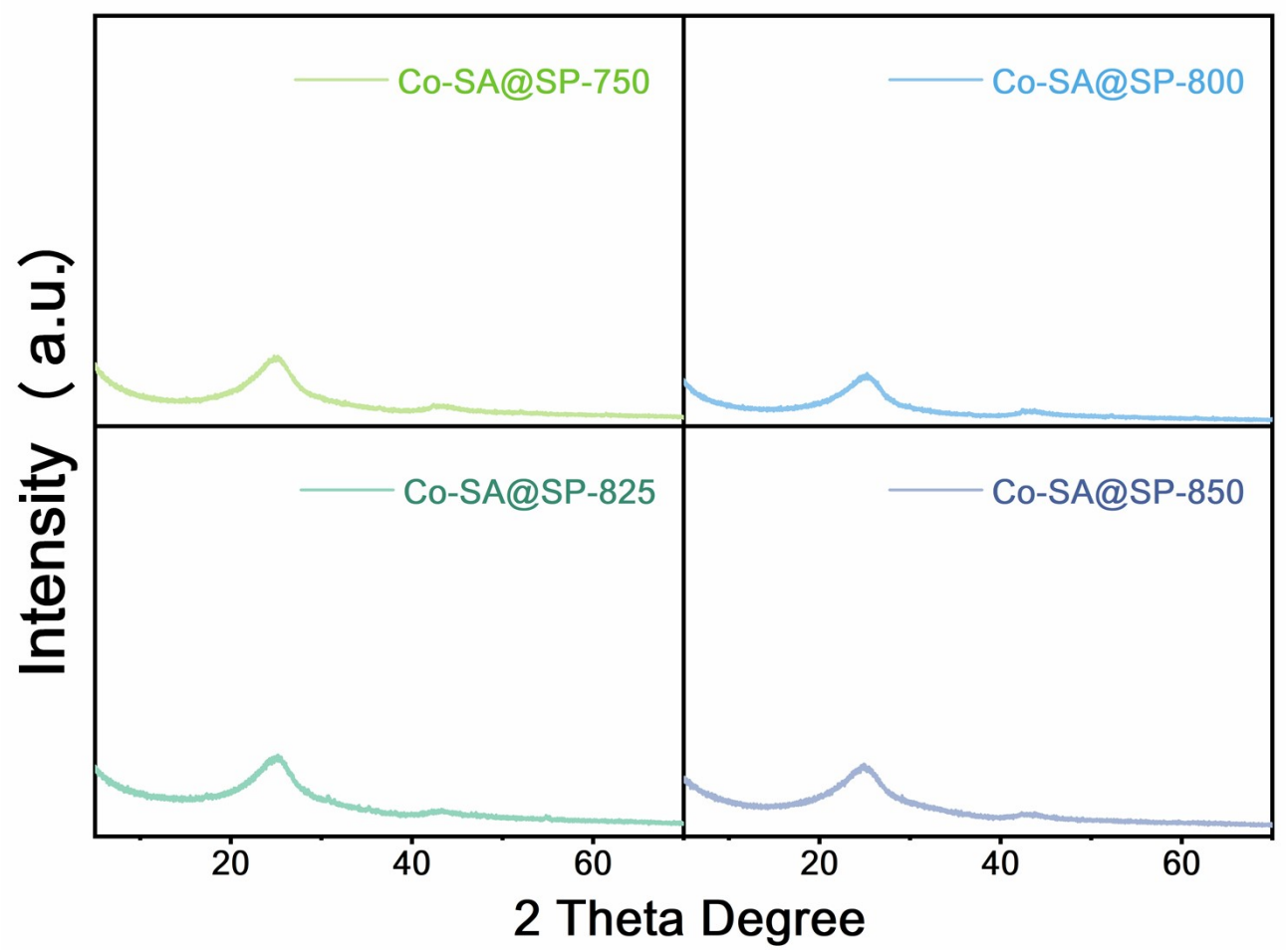

Fig. S4. XRD patterns of the Co-SA@SP-T catalysts.

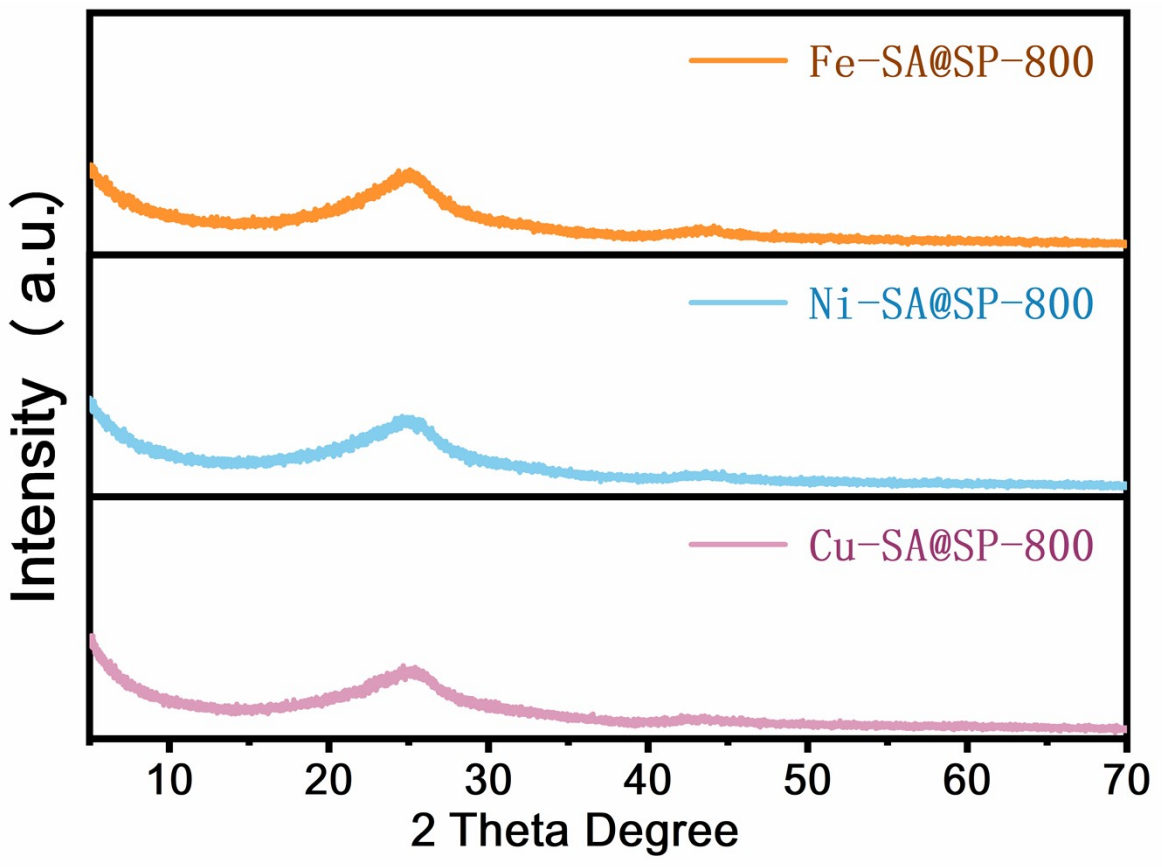

Fig. S5. XRD patterns of the M-SA@SP-800 catalysts (M = Fe, Ni, Cu, and Co).

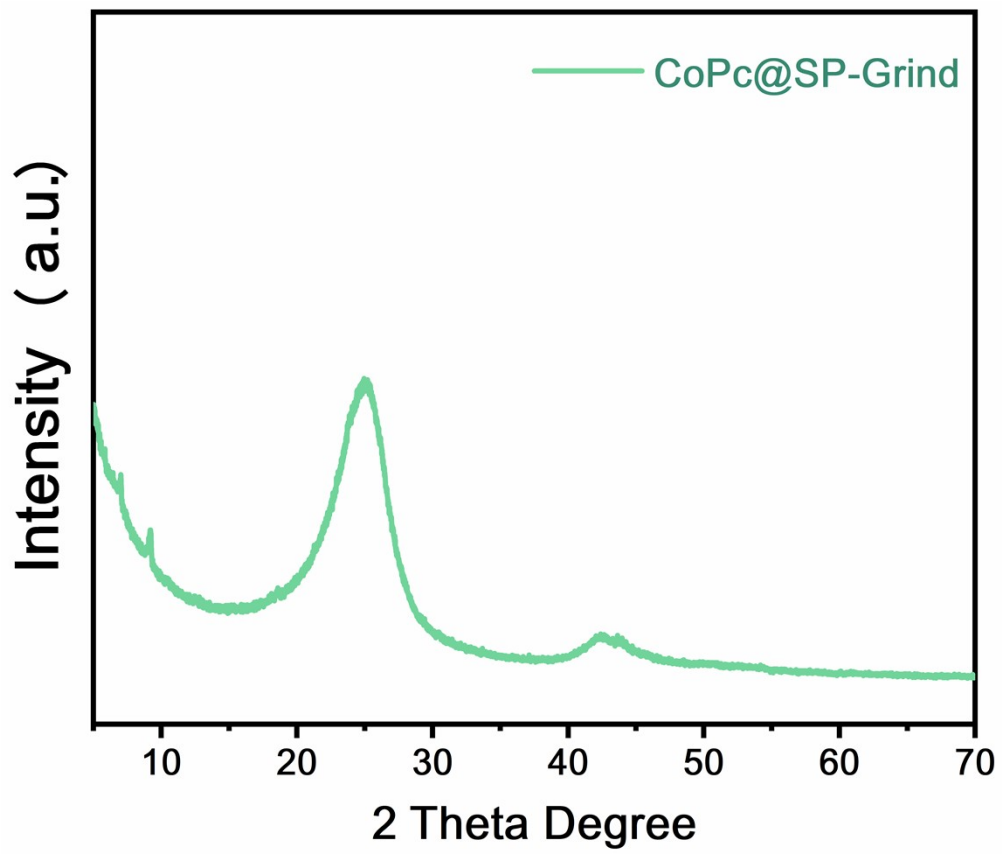

Fig. S6. The XRD pattern of the control sample of CoPc@SP-Grind.

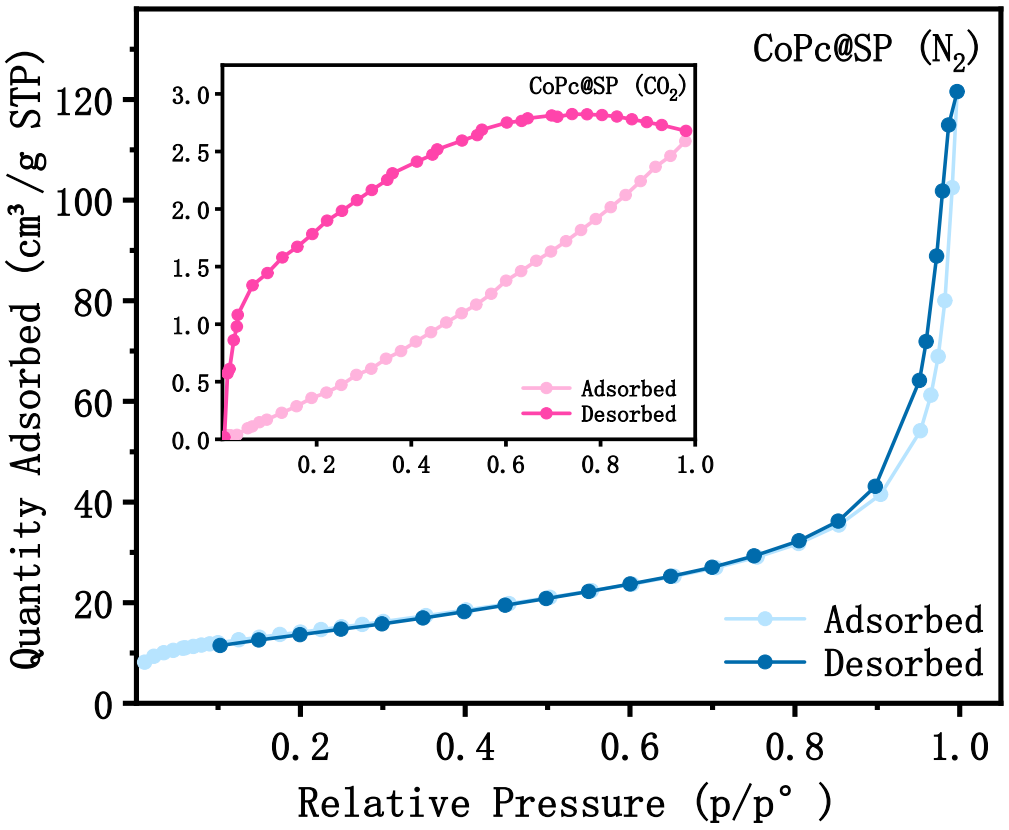

Fig. S7. N_2 adsorption-desorption isotherms of CoPc@SP. (Inset) CO_2 adsorption-desorption isotherms of CoPc@SP.

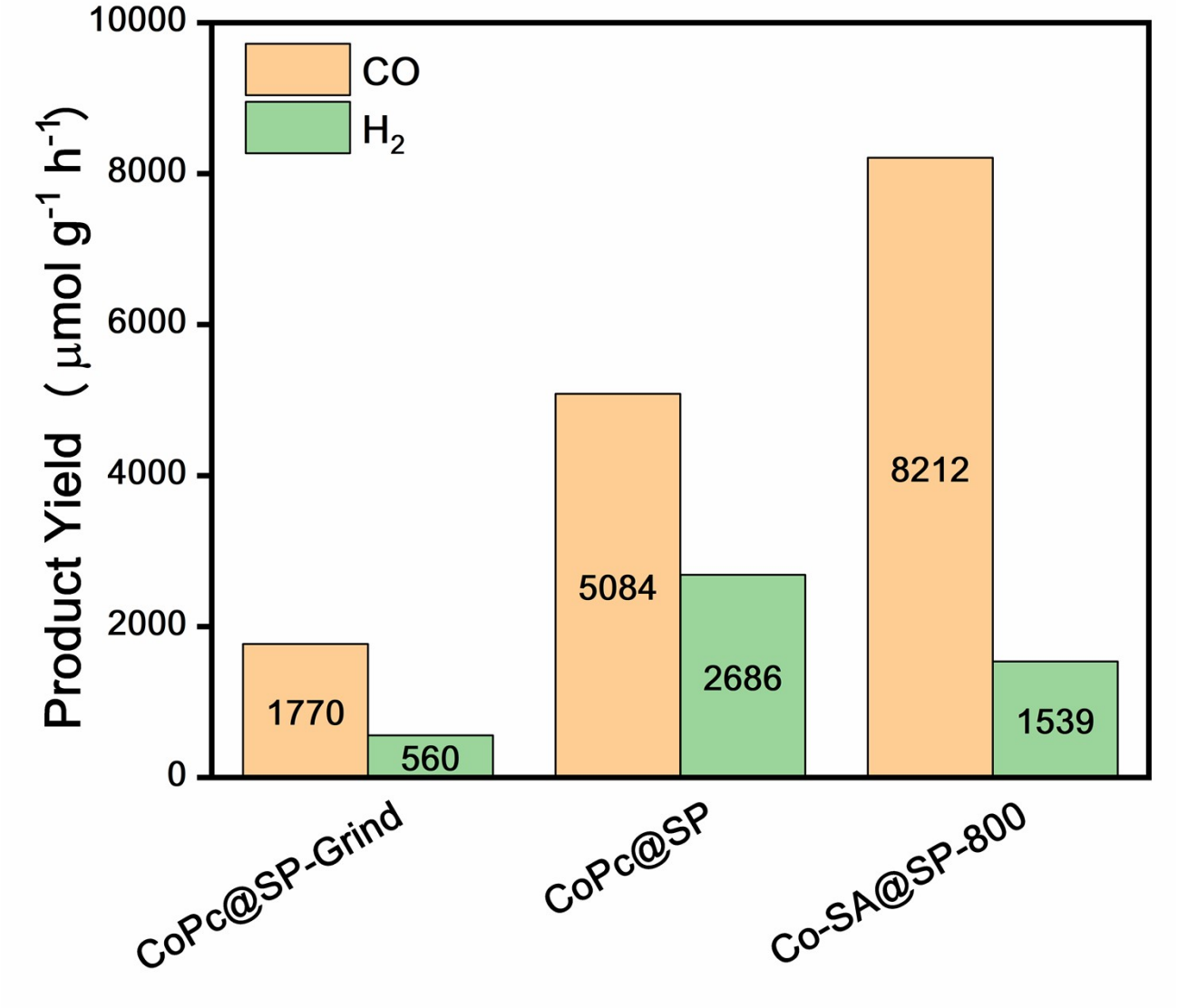

Fig. S8. The CO and H_2 yields of CoPc@SP, CoPc@SP-Grind, and Co-SA@SP-800.

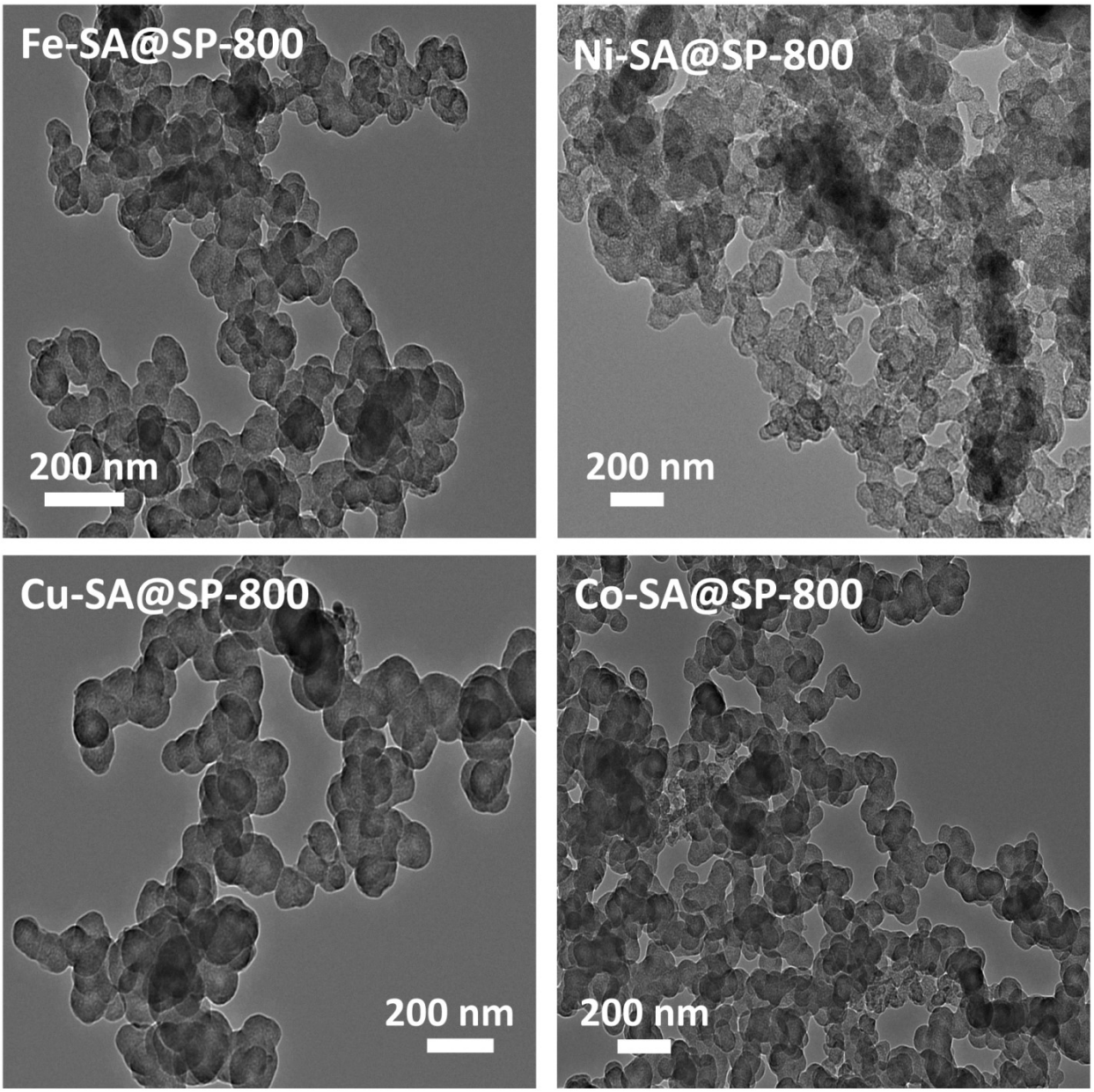

Fig. S9. TEM images of M-SA@SP-800 (M = Fe, Ni, Cu, and Co) materials.

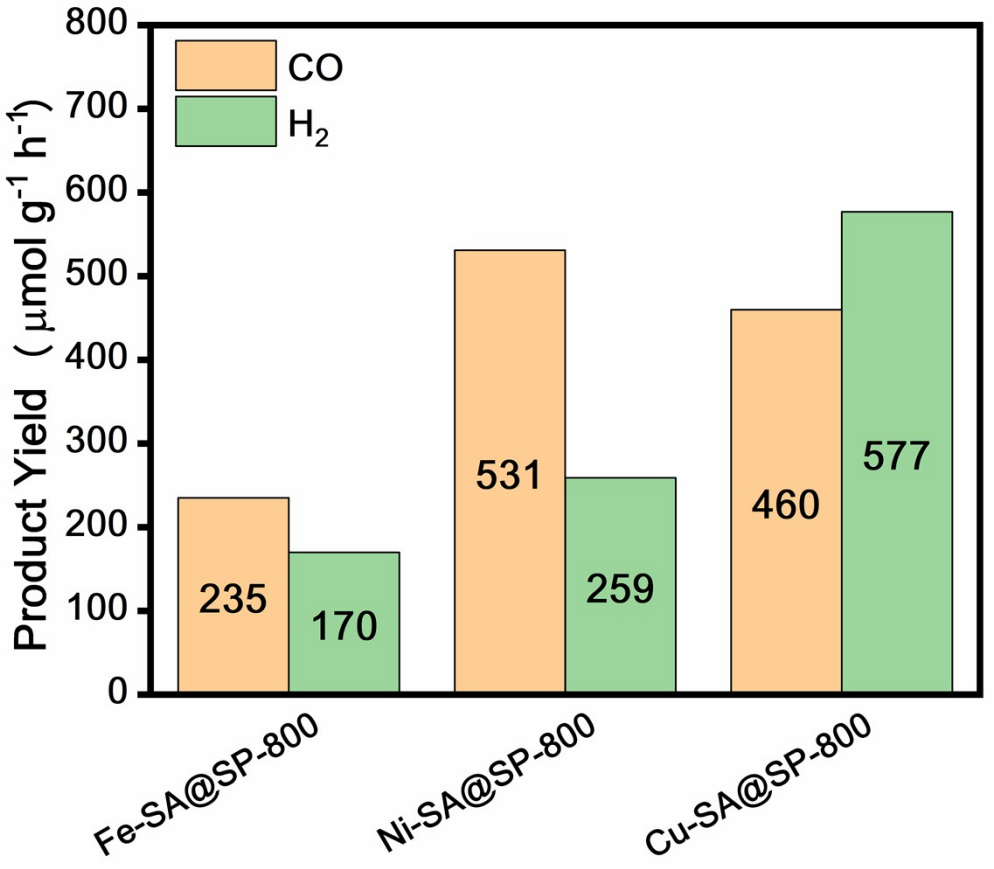

Fig. S10. The CO and H_2 yields of the M-SA@SP-800 (M = Fe, Ni, and Cu).

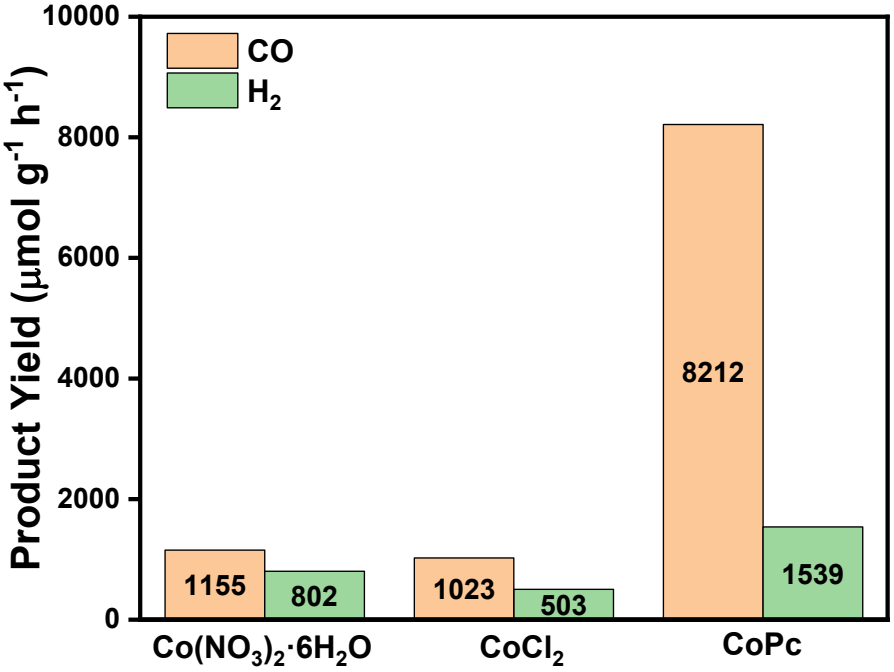

Fig. S11. The CO and H_2 yields of the Co-SA@SP-800 catalysts synthesized by using CoPc, $Co(NO_3)_2 \cdot 6H_2O$, and $CoCl_2$ as the Co source, respectively.

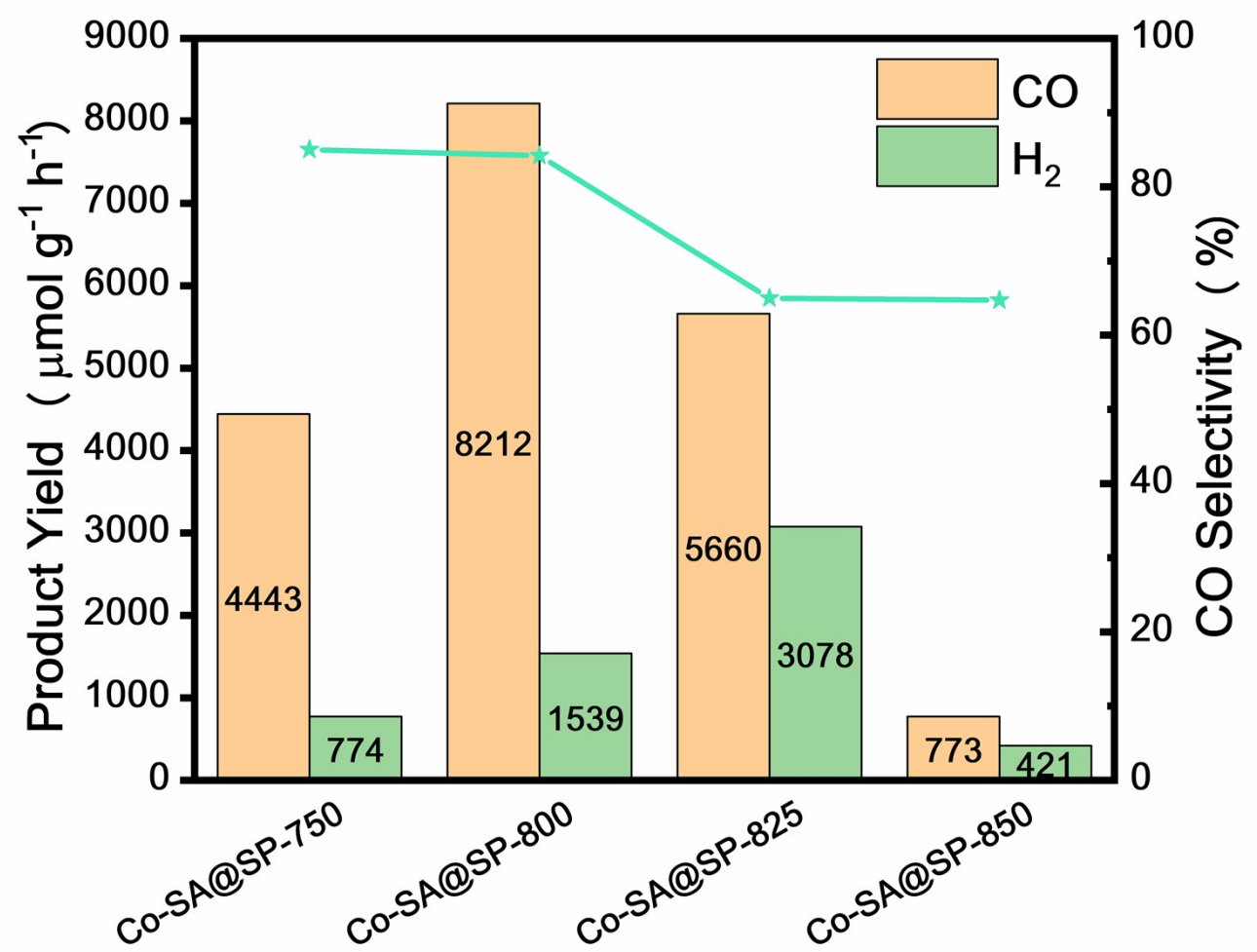

Fig. S12. The CO and H_2 yields of the Co-SA@SP-T catalysts.

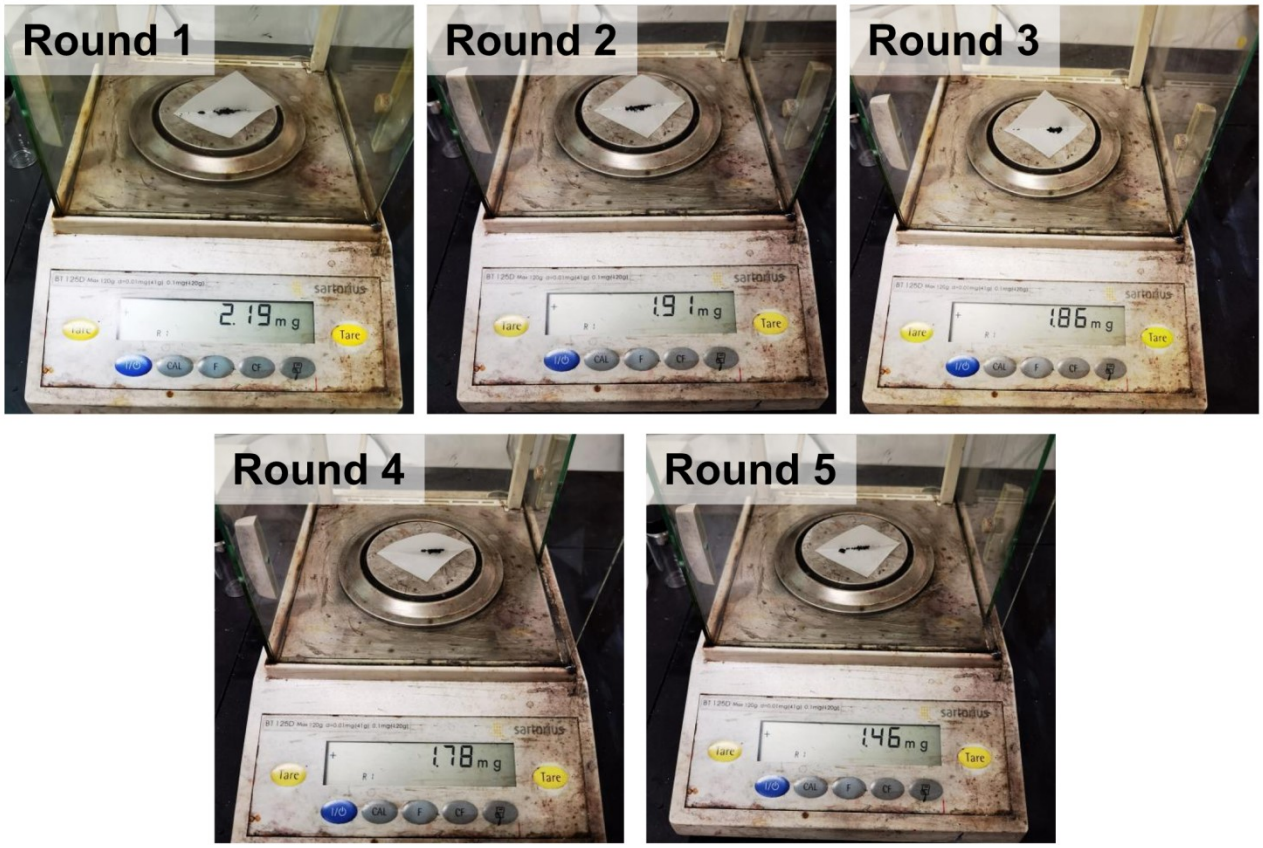

Fig. S13. Pictures of the examined catalyst weight before each round of durability test gathered by centrifuge and vacuum dry, following the order of round 1, round 2, round 3, round 4 and round 5.

Fig. S14. Picture of the heterogeneous system after photocatalytic cycling durability test.

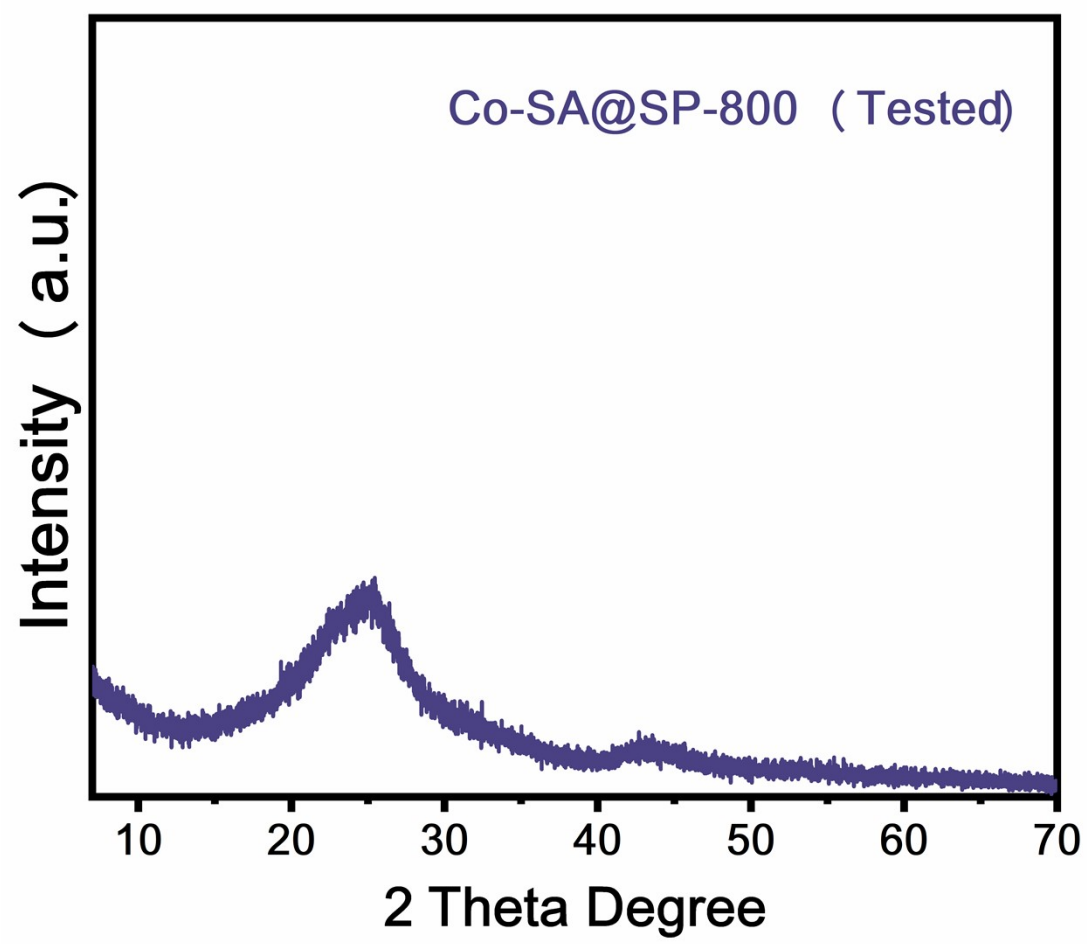

Fig. S15. The XRD pattern of Co-SA@SP-800 catalyst after stability test.

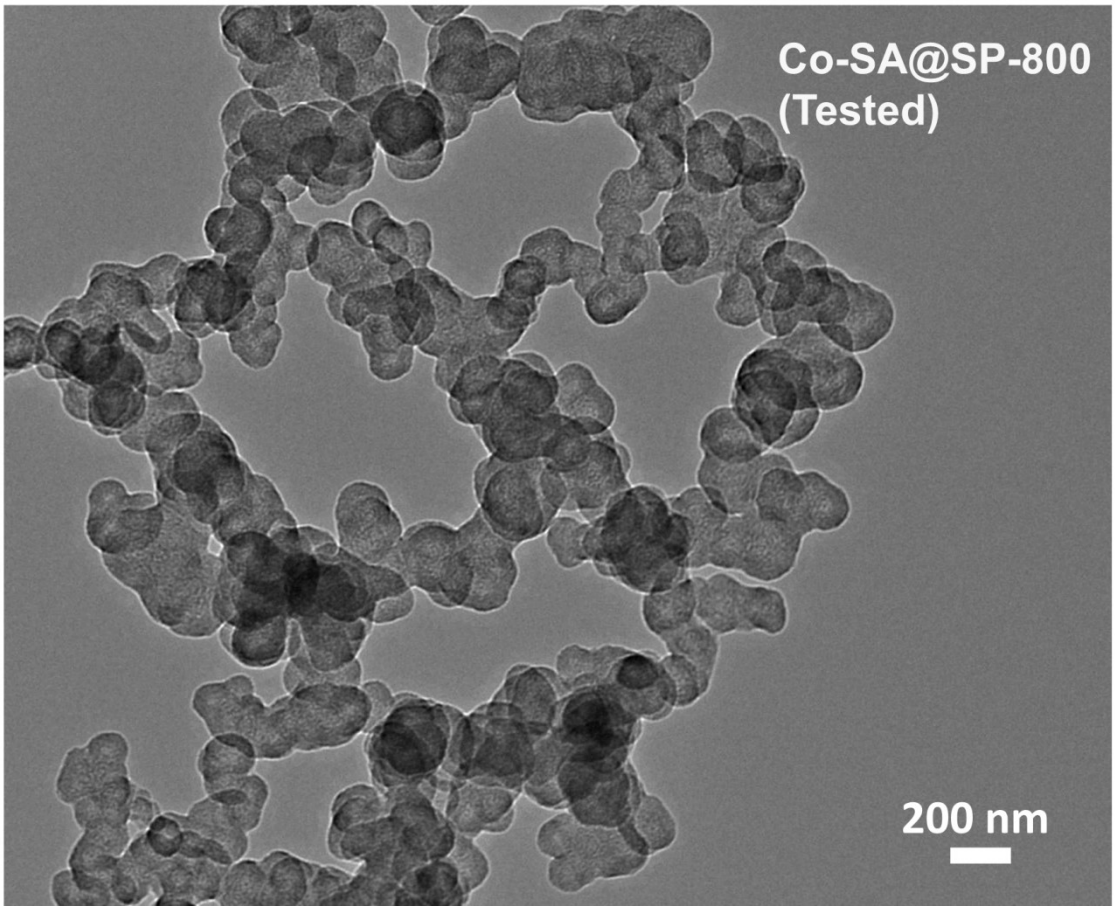

Fig. S16. The TEM image of Co-SA@SP-800 catalyst after photocatalytic cycling durability test.

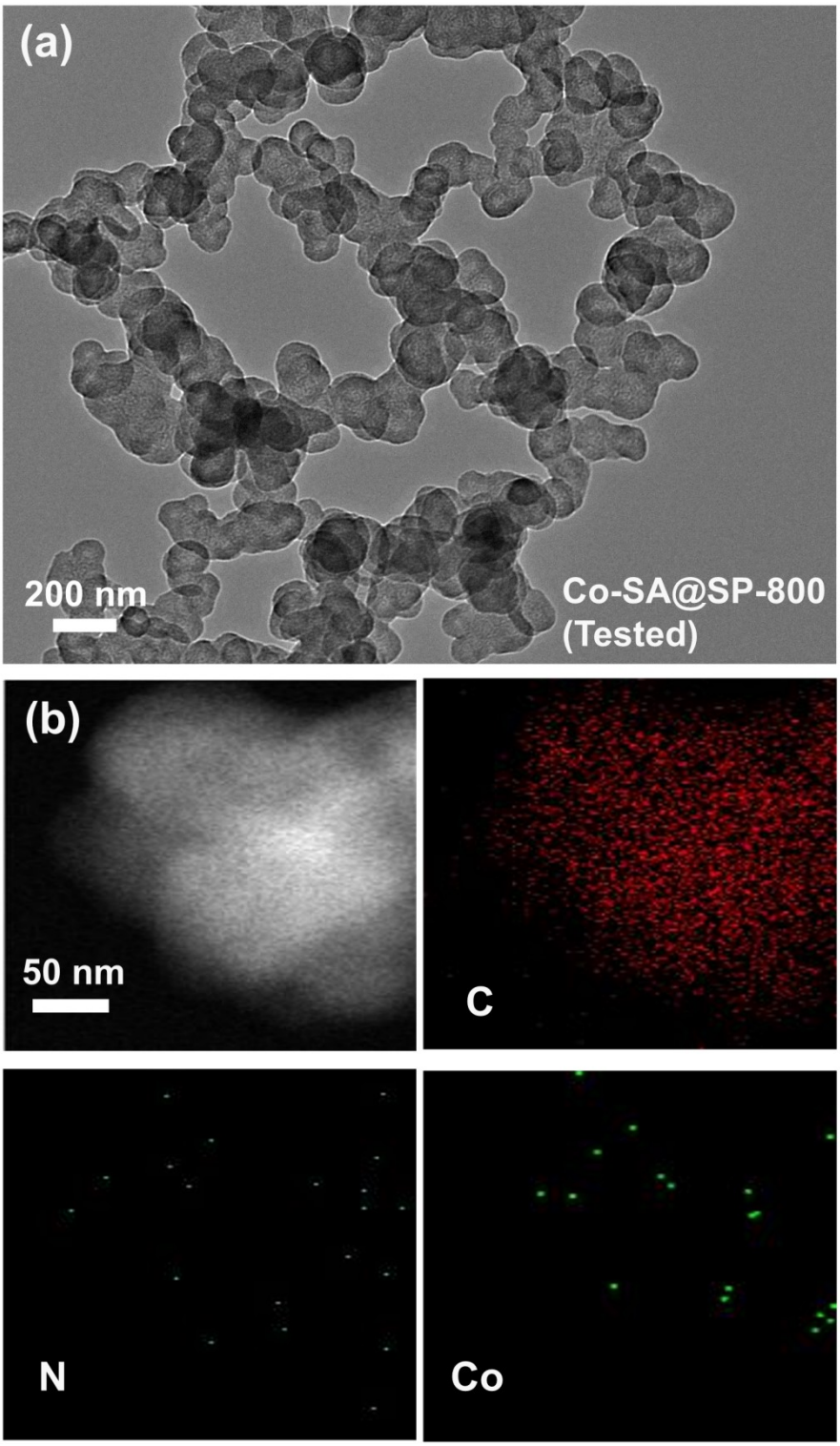

Fig. S17. The TEM, HAADF STEM and EDS images of Co-SA@SP-800 catalyst after photocatalytic cycling durability test.

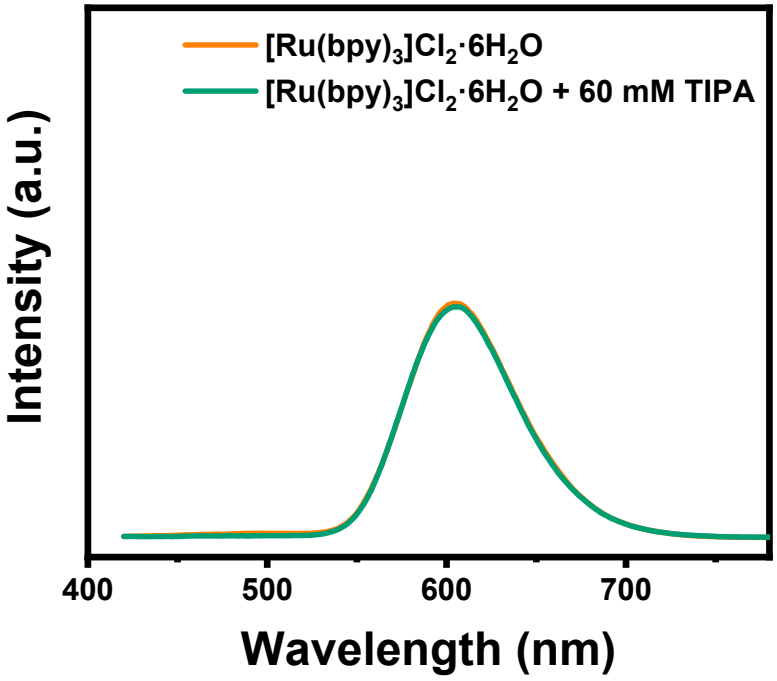

Fig. S18. PL spectra of $[Ru(bpy)_3]Cl_2 \cdot 6H_2O$ (65 μM) with different amounts of TIPA (0 and 60 mM).

Table S1. Structural parameters of Co-SA@SP-800 extracted from the EXAFS fitting. (S_0^2=0.85)

Sample	Scattering pair	CN	R(Å)	σ ^{2}(10^{-3}Å^2)	ΔE_0(eV)	R
CoN	Co-N	4.5(4)	1.94(2)	7.1 2	-3.1(3)	0.02

S_0^2 is the amplitude reduction factor; CN is the coordination number; R is interatomic distance (the bond length between central atoms and surrounding coordination atoms); σ^2 is Debye-Waller factor (a measure of thermal and static disorder in absorber-scatterer distances); ΔE_0 is edge-energy shift (the difference between the zero kinetic energy value of the sample and that of the theoretical model). R factor is used to value the goodness of the fitting.

Table S2. Main products, and their yields of several recently reported photocatalysts for photocatalytic CO_2RR, and involved equipments during the synthesis of these photocatalysts.

Catalyst	Staples	Yield	Main equipments	Ref
Co atom on Bi_3O_4Br nanosheets	CO	107.1 μmol g^{-1} h^{-1}	Teflon-lined stainless-steel autoclave	1
N-doped graphene on CdS hollow spheres	CO CH_4	2.6 μmol g^{-1} h^{-1} 0.3 μmol g^{-1} h^{-1}	Tubular furnace	2
Co atom on partially oxidized graphene nanosheets	CO	TOF - 3.77 min^{-1}	Freeze Dryer Tubular furnace	3
Ni atom on ultrathin amorphous Y_2O_3 nanosheets	CH_4	7.5 L mol m^{-2} h^{-1}	Freeze Dryer Muffle furnace	4
Pt nanoparticles on hierarchically ordered TiO_2–SiO_2 porous materials	CH_4	7.2 μmol g^{-1} h^{-1}	Muffle furnace	5
hollow nickel hydroxide nanocages	CO	1.44×10^5 μmol g^{-1} h^{-1}	Teflon-lined stainless-steel autoclave	6
Co atom on graphitic carbon nitride	CO	528 μmol g^{-1} h^{-1}	CEM Discover single-mode microwave reactor Muffle furnace	7
2,2'-bipyridine-based COF bearing single Ni sites	CO	811 μmol g^{-1} h^{-1}	Flash freezer	8

Table S3. The mass percentages of Co element in Co-SA@SP-T determined by ICP. *Percentage less than 0.5 % should be viewed as the systemic error.

Sample	Temperature (℃)	Time (h)	Co content (wt%)
Co-SA@SP-750	750	2	1.44 %
Co-SA@SP-800	800	2	1.29 %
Co-SA@SP-825	825	2	0.81 %
Co-SA@SP-850	850	2	0.59 %

3. References

1. J. Di, C. Chen, S. Z. Yang, S. Chen, M. Duan, J. Xiong, C. Zhu, R. Long, W. Hao, Z. Chi, H. Chen, Y. X. Weng, J. Xia, L. Song, S. Li, H. Li and Z. Liu, *Nat. Commun.*, 2019, **10**, 2840.
2. C. Bie, B. Zhu, F. Xu, L. Zhang and J. Yu, *Adv. Mater.*, 2019, **31**, e1902868.
3. C. Gao, S. Chen, Y. Wang, J. Wang, X. Zheng, J. Zhu, L. Song, W. Zhang and Y. Xiong, *Adv. Mater.*, 2018, **30**, e1704624.
4. Y. Li, J. Hao, H. Song, F. Zhang, X. Bai, X. Meng, H. Zhang, S. Wang, Y. Hu and J. Ye, *Nat. Commun.*, 2019, **10**, 2359.
5. C. Dong, C. Lian, S. Hu, Z. Deng, J. Gong, M. Li, H. Liu, M. Xing and J. Zhang, *Nat. Commun.*, 2018, **9**, 1252.
6. Y. Su, Z. Song, W. Zhu, Q. Mu, X. Yuan, Y. Lian, H. Cheng, Z. Deng, M. Chen, W. Yin and Y. Peng, *ACS Catal.*, 2020, **11**, 345-354.
7. P. Huang, J. Huang, S. A. Pantovich, A. D. Carl, T. G. Fenton, C. A. Caputo, R. L. Grimm, A. I. Frenkel and G. Li, *J. Am. Chem. Soc.*, 2018, **140**, 16042-16047.
8. W. Zhong, R. Sa, L. Li, Y. He, L. Li, J. Bi, Z. Zhuang, Y. Yu and Z. Zou, *J. Am. Chem. Soc.*, 2019, **141**, 7615-7621.